Possible half-metallic behavior of $Co_{2-x}Cr_xFeGe$ Heusler alloys: Theory and experiment

R. Mahat,[1,*] S. KC,[1] U. Karki,[1] J. Y. Law,[2] V. Franco,[2] I. Galanakis,[3] A. Gupta,[4] and P. LeClair[1,†]

[1]*Department of Physics and Astronomy, The University of Alabama, Tuscaloosa, Alabama 35487, USA*

[2]*Departmento de Física de la Materia Condensada ICMSE-CSIC, Universidad de Sevilla, Sevilla 41080, Spain*

[3]*Department of Materials Science, School of Natural Sciences, University of Patras, GR-26504 Patras, Greece*

[4]*Department of Chemistry and Biochemistry, The University of Alabama, Tuscaloosa, Alabama 35487, USA*

(Received 14 October 2020; accepted 8 July 2021; published 28 July 2021)

This paper reports a combined experimental and theoretical study of structural, electronic, magnetic, and mechanical properties of quaternary Heusler alloys $Co_{2-x}Cr_xFeGe$ prepared by arc-melting with Cr concentrations $0 \leqslant x \leqslant 1$. Single-phase microstructures are observed for Cr compositions from $x = 0.25$ to $x = 1$. Lower Cr concentrations are multiphased. X-ray diffraction patterns at room temperature reveal a face-centered cubic crystal structure in all single-phase samples. The low-temperature saturation magnetic moments, as determined from magnetization measurements, agree fairly well with our theoretical results and also obey the Slater-Pauling rule for half-metals, a prerequisite for half-metallicity. All alloys are observed to have high Curie temperatures that scale linearly with the saturation magnetic moments. Relatively high mechanical hardness values are also observed. First-principles calculations also predict a finite band gap in the minority spin channel of the alloys, increasing in size with increasing Cr concentration. Cr substitution brings the Fermi level toward the center of this gap while also increasing the majority spin density of states near the Fermi level. As a whole, $Co_{2-x}Cr_xFeGe$ shows great promise as a half-metal with 100% spin polarization.

DOI: 10.1103/PhysRevB.104.014430

I. INTRODUCTION

Heusler alloys consist of a large family of intermetallic compounds exhibiting varieties of magnetic phenomena. Recently, the interest has been focused on those having half-metallic character for their potential use in magneto-electronic devices [1]. Co_2-based full Heusler compounds with stoichiometric composition Co_2YZ, (Co,Y) being two transition metals, and Z being main group element, crystallizing in the $L2_1$ structure (space group $Fm\bar{3}m$, No. 225 [2,3]) belong to the most promising candidates of this family scientifically and technologically [4–14]. These materials exhibit high Curie temperature (T_c), varying magnetic moments ranging from 0.3 μ_B to 1.0 μ_B at the Co site (depending on the constituents Y and Z), compatible lattice mismatch with conventional semiconductors, and 100% spin polarization at room temperature, arising from the exceptional electronic structure with an energy band gap at the Fermi level (E_F) for minority spin subband [1,6,15–19].

However, the experimentally observed spin polarization values of most of the Co_2-based ternary Heusler alloys are always much smaller than the theoretical values. The discrepancy between theory and experiment is expected due to the structural disorder in the crystal lattices [9,20]. In many cases, improvements in various properties such as structure, magnetization, transport, critical temperature T_c, magnetoresistance, as well as high spin polarization are realised in slightly disordered Heusler alloys by the substitution of a quaternary element, as quaternary element additions are observed to reduce the structural disorder and change the degree of hybridization between the 3*d* orbitals of different elements with consequent changes in the position of the Fermi level with respect to the spin subband [21–26]. Özdoğan *et al.* [27] have done the theoretical study of the doping effect of low-valent transition metal atoms in ternary Heusler alloys. They have observed the change in electronic structure opening the energy gap around Fermi level in minority states by electron doping, which gives 100% spin polarization, stabilizing the half-metallic character. So, doping is considered as one of the promising ways to stabilize Co_2-based new robust half-metals [28].

The Co_2FeGe (CFG) system is of interest in spintronic applications due to its high Curie temperature and is predicted theoretically to be stable, crystallizing in the $L2_1$ structure with Fermi level falling on the edge of the minority conduction band making the system shy from being half-metallic, but it is observed experimentally to show multi-phase behavior in bulk form [29–31]. High $T_c = 981$ K and large magnetic moment of 5.74 μ_B/f.u. for disordered CFG is reported in Ref. [30]. Balke *et al.* [32] have observed CFG to crystallize in $L2_1$ structure by analyzing the EXAFS data. While quaternary Heusler alloy CoFeCrGe (CFCG) is observed theoretically and experimentally to be nearly half metallic with Fermi level falling on the edge of the minority valence band, leading to an unstable half-metallicity [33–36]. So, as we go from CFG to CFCG, Fermi level is shifted from lower edge of conduction band to upper edge of valence band in minority spin channel, which is in accordance to the calculations by

*rmahat@crimson.ua.edu

†pleclair@ua.edu

Galanakis *et al.* [37]. They have suggested that an expansion of the lattice should shift the Fermi level deeper in energy and the contraction should shift it higher in energy. Therefore, one can expect robust half-metallicity with Fermi level exactly at the middle of the band gap for some intermediate Cr concentrations in CFG due to the expansion of the lattice when Cr with larger atomic radius substitutes for Co [38]. The substitution of Cr to Co may be also seen as *d*-electron deficiency.

There are some successful reports on CFG system where substitution plays an important role to stabilize the $L2_1$ phase and tune the Fermi level towards the minority band gap. The band gap at the Fermi level can be tuned by substituting a fourth element at X/Y/Z site, i.e., $Co_{2-x}Y^*_xYZ$, $Co_2Y_{1-x}Y^*_xZ$, or $Co_2YZ_{1-x}Z^*_x$, where Y, Y* are low valent transition elements and Z, Z* are main group elements [20,39–44]. The substitution at X/Y site is more convincing as X/Y site element plays main role in tailoring the half-metallicity and magnetic properties compared to Z site [37]. Ti substitution for Co in disordered CFG is reported to stabilize the system and tune the Fermi level towards the middle of the band gap [31]. Venkateswarlu *et al.* [45] were able to obtain the stable $L2_1$ phase in $Co_2Ti_{1-x}Fe_xGe$ substitutional series in bulk form with some antisite disorder. Varaprasad *et al.* [26] were able to measure spin polarization as high as 0.69 in CFG by substituting Ga for Ge, i.e., $Co_2Fe(Ga_{1-x}Ge_x)$. All these approaches have inspired us to synthesize CFG, a potential candidate for spintronic applications, and investigate the effect of Cr substitution for Co in CFG on structural, electronic, magnetic, and mechanical properties. In particular, we present results on the extent to which Cr can help to tune the half-metallic character stabilizing the $L2_1$ structure in $Co_{2-x}Cr_xFeGe$ Heusler system.

II. METHODS

A. Experimental methods

The bulk $Co_{2-x}Cr_xFeGe$ $(0 \leqslant x \leqslant 1)$ stoichiometric Heusler alloys were prepared by melting Co, Fe, Cr, and Ge pieces of 99.99% purity in an arc furnace on a Cu hearth provided with water cooling under argon flow at a base pressure of 10^{-4} mbar. The mixture was melted at least 6 times to ensure chemical homogeneity. As an oxygen getter, Ti was melted inside the vacuum chamber separately before melting the compound to avoid oxygen contamination. The weight loss during the process was negligible. The resulting ingots were cut into pieces and examined using an energy dispersive x-ray spectroscopy (EDS) detector equipped in a JEOL 7000 field emission scanning electron microscope (FESEM) to ensure the target composition after the arc melting. These pieces were annealed in evacuated quartz tubes for different heat treatments, and cooled slowly in the furnace to get optimum crystallization to promote the formation of $L2_1$ structure. To make the comparison uniform across all compositions, only the samples annealed under similar heat treatments (i.e., 1000 °C for 15 days) are reported. The heat treatments were followed by metallography (see details in the Supplemental Material [46]) to produce a metallic shiny surface for microstructure analysis by optical and electron microscopes. After the heat treatment and metallography, the composition and homogeneity of the samples were again confirmed by using EDS.

Structural analysis was carried out by using x-ray diffraction (XRD) using a Bruker D8 Discover x-ray diffractometer equipped with monochromatic Co-Kα ($\lambda = 0.179$ nm) radiation. The polished samples were rotated around the ϕ axis during the XRD measurement to minimize surface effects. CARINE crystallography 4.0 software [47] as well as in-house PYTHON code [48] including the dispersive corrections to the atomic scattering factors were used to simulate the XRD patterns to compare with the experimental XRD patterns. Rietveld refinement was done using a MATCH! software based on the FULLPROF algorithm [49]. The low-temperature magnetic properties were studied in Quantum Design Physical Properties Measurement System (PPMS), while the high-temperature magnetization was measured using LakeShore VSM 7407. The mechanical properties were studied in terms of Vickers hardness by using Buehler model 1600-6100 micro-hardness tester.

B. Computational methods

We have performed density functional theory (DFT) calculations employing the projector augmented wave (PAW) pseudopotentials by Blöchl [50], implemented by Kresse and Furthmüller in the Vienna *ab initio* simulation package (VASP) [51]. We have adopted the generalized gradient approximation (GGA) in the scheme of Perdew, Burke, and Ernzerhof (PBE) for the electronic exchange-correlation functional [52]. We have used a 16-atom supercell, i.e., 4 formula units of the underlying $L2_1$ structure adopted by the perfect full-Heusler compounds like Co_2MnGe. The integration over the irreducible Brillouin zone (IBZ) of cubic systems was done with the automatic mesh generation scheme within VASP with the mesh parameter (the number of k points per $Å^{-1}$ along each reciprocal lattice vector) set to 30, which generates a $10 \times 10 \times 10$ Γ-centered Monkhorst-Pack grid in the case of cubic lattices [53]. Total energies were converged upto 10^{-7}eV/cell with a plane-wave cutoff of 520 eV. Full relaxation of cell (initially cubic) volume, shape and atomic positions were performed until the forces on each atom become less than 10^{-2} meV/cell using the conjugate-gradient method. Our calculations did not include spin-orbit interaction but the latter is not crucial for the half-metallic properties of Heusler compounds [54].

III. RESULTS AND DISCUSSIONS

A. Experimental results and discussions

1. Microstructural and compositional analysis

XRD can not detect additional phases when the impurity phase contents are either below the detection limit of XRD (less than roughly 5% of the overall volume) or amorphous in nature [31,55,56]. In such case, optical microscopy and SEM of polished and etched samples are the most direct ways to characterize the microstructure because they give a morphological image, which can clearly figure out secondary phases and grain boundary segregation even for minor constituents. Observing different contrast in etched sample seen from

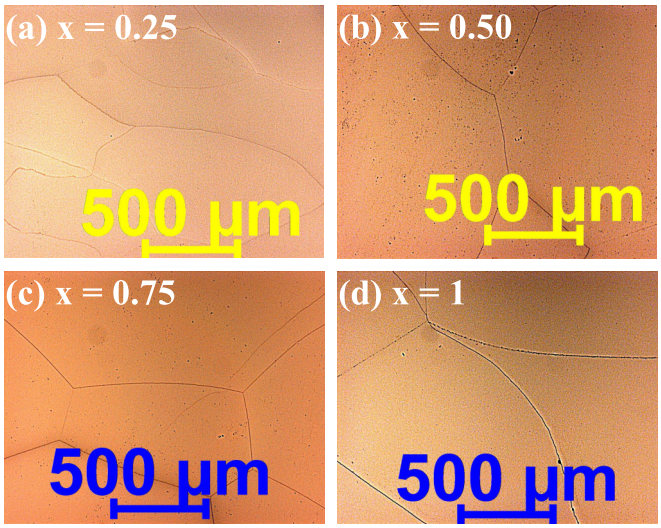

FIG. 1. Optical micrograph of $Co_{2-x}Cr_xFeGe$ annealed at 1000 °C for 15 days followed by slow cooling showing the granular microstructure. The samples were etched for 30 seconds using the Adler etchant.

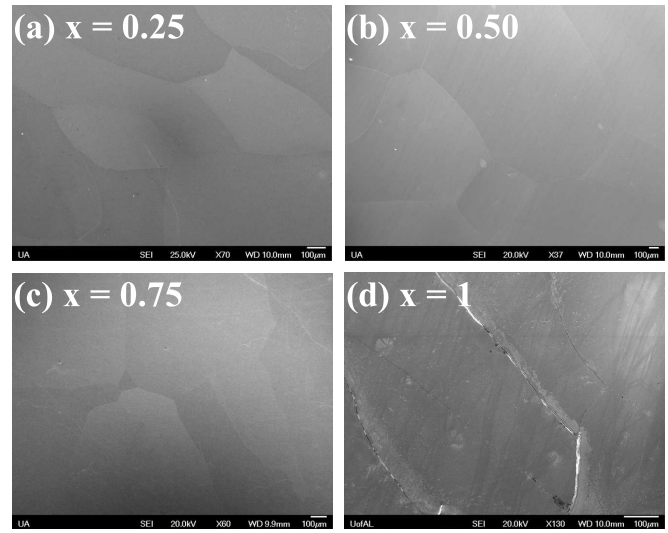

FIG. 2. SEM micrograph of $Co_{2-x}Cr_xFeGe$ annealed at 1000 °C for 15 days followed by slow cooling showing the granular microstructure.

optical microscopy, we can speculate the presence of impurity phases, and SEM with EDS can be used to directly quantify whether areas of different contrasts represent impurity phases or possible different crystallite orientations.

In accordance with previous reports of the full stoichiometric CFG [29–31,57], multiphase microstructure was obtained for all the heat treatments performed at 900, 950, or 1000 °C for different dwelling times; 3, 7, or 15 days. However, with the substitution of Cr for Co, there is a rapid conversion of this multiphase microstructure toward a single-phase microstructure for the samples annealed at 1000 °C for 15 days in the composition range ($0.25 \leqslant x \leqslant 1$). Low Cr concentration ($x < 0.25$) produced multiphase behavior. Figure 1 shows the microstructure of all single-phase samples observed using optical microscope. The contrast developed in micrograph (see details in the Supplemental Material [46]) suggests significant compositional differences between phases in the case of parent CFG ($x = 0$). The composition was measured to differ from the target composition by more than 5% with the secondary phase mainly located in grain boundaries and same trend is observed with the chromium substitution $x = 0.125$ in place of Co, though the major granular phase was identified to be close to target and nominal secondary phase was observed to segregate in grain boundaries, which can also be seen from elemental mapping images of constituent elements in homogenized $Co_{2-x}Cr_xFeGe$ alloys presented in the Supplemental Material [46]. The stoichiometry within the grains of all the single-phase samples was confirmed as the target composition within an instrumental uncertainty of $\sim 5\%$ using EDS. Typical SEM images displaying the microstructure of single-phase samples are shown in Fig. 2. Relatively large grains are observed.

2. *Crystal structure and atomic order analysis*

Structural characterization has been performed with XRD as the standard method. Although, XRD suffers from some limitations due to very small differences in the atomic scattering factors between constituent transition elements in $Co_{2-x}Cr_xFeGe$, an important structural information concerning atomic disorder can be obtained from the analysis of the relative intensities of the superstructure reflection peaks (111) and (200). Figure 3 shows the XRD patterns for $Co_{2-x}Cr_xFeGe$ alloys annealed at 1000 °C for 15 days, measured at room temperature, using a Co-K_α radiation source. Single-phase behavior can be seen only for $0.25 \leqslant x \leqslant 1$ while low Cr concentrations are multiphase (impurity peaks are represented by asterisks). Simple structural information of a cubic single phase can be gained by indexing all XRD peaks. For all cubic single-phase compositions, only three distinct Heusler-like reflection peaks (h, k, l all odd or even) are observed; fundamental peaks with $h + k + l = 4n$, even superlattice peaks with $h + k + l = 4n + 2$ and odd superlattice peaks with $h + k + l = 2n + 1$. Heusler alloys in the ordered $L2_1$ structure are characterized by the presence of superlattice diffraction peaks; the presence of (111) peak indicates the chemical ordering of atoms in octahedral positions, and (200) peak indicates the order for atoms in tetrahedral positions, while (220) peak is a principal reflection, which is independent of the state of the order [58].

In full Heusler alloys (FHA) of the type X_2YZ, transition metal atoms X are of the intermediate electronegativity values and occupy 8c($\frac{1}{4}$, $\frac{1}{4}$, $\frac{1}{4}$) [or 4c($\frac{1}{4}$, $\frac{1}{4}$, $\frac{1}{4}$), and 4d($\frac{3}{4}$, $\frac{3}{4}$, $\frac{3}{4}$)], the low-valence transition metal atom Y with least electronegativity occupies 4b($\frac{1}{2}$, $\frac{1}{2}$, $\frac{1}{2}$), and the most electronegative main group element Z occupies 4a(0,0,0) Wyckoff positions of the space group $Fm\bar{3}m$ [9,59]. Here, we refer 4a and 4b sites as A sublattice and 4c and 4d as B sublattice as shown in Fig. 6. If one X is replaced by a different transition metal X′, a quaternary Heusler structure (or Y structure) with different symmetry (space group $F\bar{4}3m$ No. 216) is obtained and written as XX'YZ. In the present system under study, one can expect a change in structural order from $L2_1$ ($x = 0$) to Y structure ($x = 1$) after Cr substitution, as the parent alloy CFG

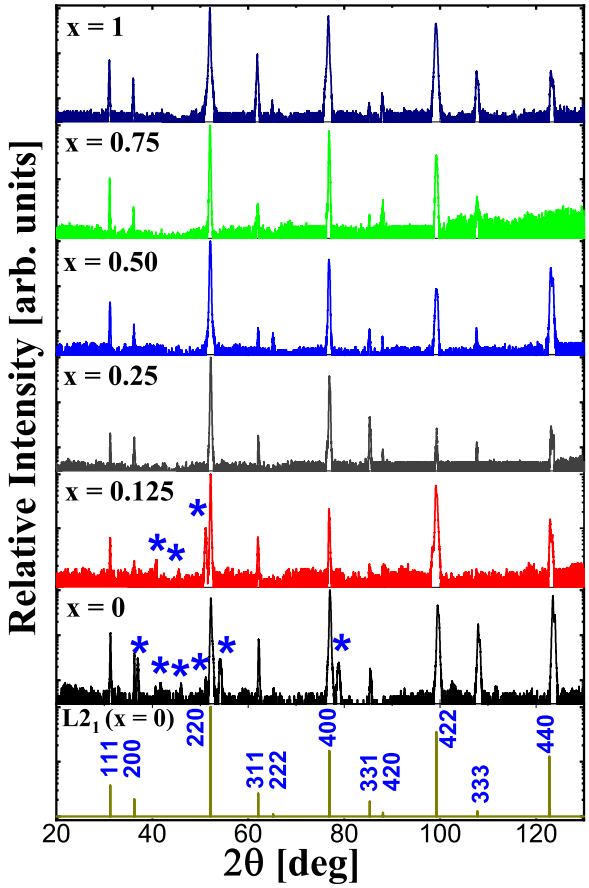

FIG. 3. Experimental XRD patterns of $Co_{2-x}Cr_xFeGe$ alloy series annealed at 1000 °C for 15 days investigated at room temperature; here, ∗ corresponds to the secondary phase/unknown impurity phase. The first from the bottom is the simulated XRD pattern for ordered $L2_1$ structure of CFG. The relative intensity (y axis) is plotted in log scale so that all the peaks can be seen clearly.

($x = 0$) has been reported to crystallize in $L2_1$ structure with some disorder [26,29,30]. The intensities of superstructure peaks are sensitive to different kinds of atomic disorders, e.g., (i) A2-type disordered structure with vanishing superstructure peaks when all the atoms are randomly distributed over lattice sites 4a, 4b, 4c, and 4d; (ii) disordered $L2_1$ structure (like B2-type in FHA) with only the (200) superstructure peak and vanishing (111) peak when there is a disorder between atoms in 4a and 4b sites; and (iii) DO_3 type when disorder is between atoms in 4b, 4c, and 4d sites only [36]. This disordered structure DO_3 results (111) superstructure peak with much higher intensity than the (200) peak. All these types of disorder induce states at the edges of the minority-spin band gap leading eventually to the loss of half-metallicity for a critical value of disorder, the later being specific and depending on the kind of disorder [43]. In such cases, the magnetic moments may still follow a Slater-Pauling rule.

We present the enlargement of the experimental XRD patterns between 29.5° and 37° for single-phase samples to clearly show the superlattice reflections (111) and (200) in Fig. 4(a) with corresponding simulated patterns of ideal $L2_1$ structure (Y structure for $x = 1$) for comparison in Fig. 4(b); the two diffraction peaks are clearly visible as expected

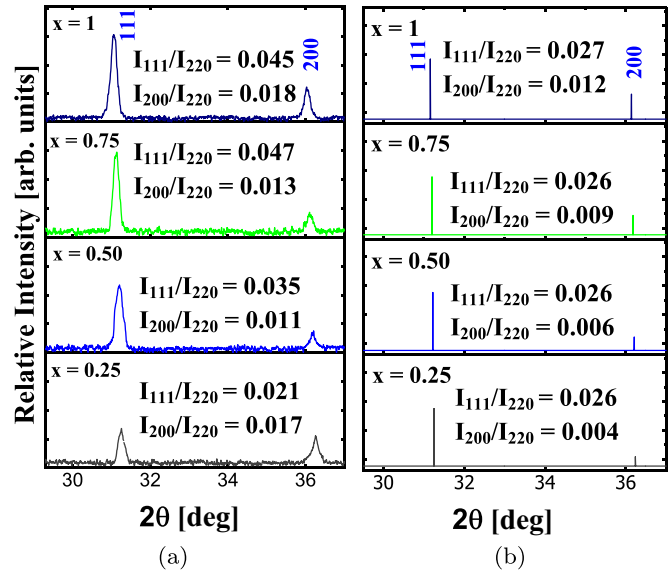

FIG. 4. (a) Enlargement of (111) and (200) x-ray diffraction peaks of single-phase samples and (b) the corresponding simulated patterns for the ideal ordered structure.

for the defect-free ordered Heusler structure, indicating the presence of a long range ordering in these samples. The measured and expected I_{111}/I_{220} and I_{200}/I_{220} are also labeled. These values agree with each other qualitatively. Due to the small differences in the atomic scattering factors between the constituent $3d$ metals in $Co_{2-x}Cr_xFeGe$ and the unknown degree of texturing in the samples, which might alter the relative intensity of XRD peaks, it is difficult to identify the exact chemical ordering. Therefore, we performed Rietveld refinement of experimental XRD pattern for $x = 0.50$, i.e., $Co_{1.50}Cr_{0.50}FeGe$ considering four nondegenerate configurations. Further detail about other possible chemical orderings will be discussed in the forthcoming theoretical section. These four nondegenerate configurations and corresponding goodness of fit parameters for $x = 0.50$ are shown in Table I. Figure 5 shows the observed, calculated, and difference profiles for the best fit configuration (I) after performing the Rietveld refinement. The crystal structure for this configuration is shown in Fig. 6(b) (see the Supplemental Material [46] for crystal structures for other possible configurations). In this configuration, the Ge atoms occupy the 4a position, a statistical distribution of the Fe and the Cr, which substitute Co atoms in the chemical formula is expected at 4b, the Fe atoms initially at these site in the perfect $L2_1$ structure migrate

TABLE I. Possible site assignments for cubic $Co_{2-x}Cr_xFeGe$ with corresponding goodness of fit parameter for $x = 0.50$.

Type	4a (0,0,0)	4b $(\frac{1}{2},\frac{1}{2},\frac{1}{2})$	4c $(\frac{1}{4},\frac{1}{4},\frac{1}{4})$	4d $(\frac{3}{4},\frac{3}{4},\frac{3}{4})$	$\chi^2_{x=0.50}$
I	Ge	$Fe_{1-x}Cr_x$	$Co_{1-x/2}Fe_{x/2}$	$Co_{1-x/2}Fe_{x/2}$	1.1
II	Ge	$Fe_{1-x}Cr_x$	$Co_{1-x}Fe_x$	Co	1.7
III	Ge	$Co_{1-x}Cr_x$	Fe	Co	1.9
IV	Ge	Fe	$Co_{1-x}Cr_x$	Co	2.2

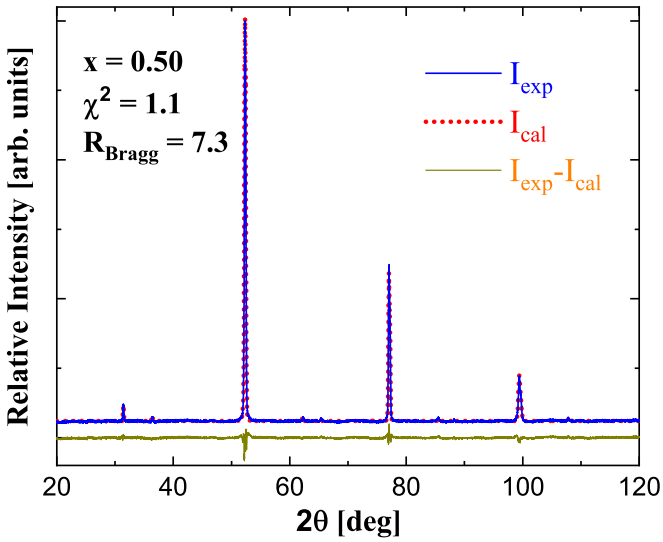

FIG. 5. Rietveld refinement performed on $Co_{1.50}Cr_{0.50}FeGe$ annealed at 1000 °C for 15 days followed by slow cooling considering first atomic configuration given in Table I.

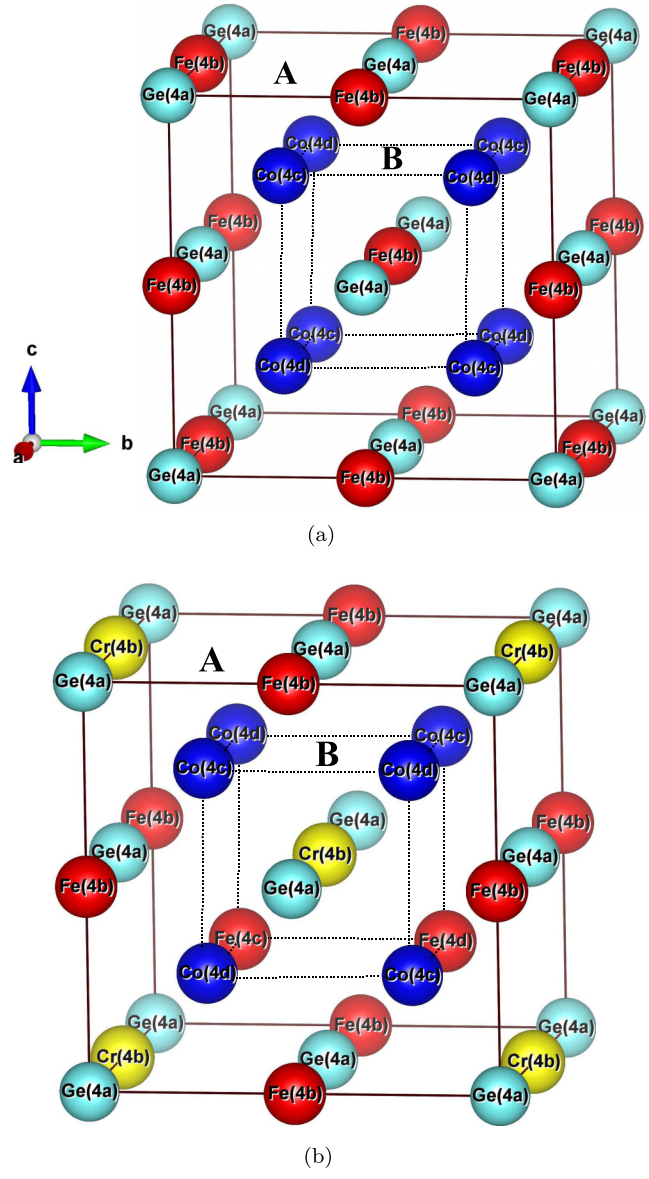

FIG. 6. Crystal structure in unit cell of (a) CFG and (b) $Co_{1.50}Cr_{0.50}FeGe$ (I) configuration mentioned in Table I assuming $L2_1$ structure. The structures are shown in their ideal, unrelaxed forms.

to the tetrahedral sublattice B initially occupied purely by Co, i.e., Co and Fe are on the tetrahedral sublattice B (4c and 4d) and Fe, Cr, and Ge on the octahedral sublattice A (4a and 4b). In $Co_{2-x}Cr_xFeGe$, Cr is the least electronegative (1.66 Pauli units) [60]. Therefore, we presume that Cr substitution will displace the Fe atoms towards vacated Co sites and it will fill the site previously occupied by Fe forming an ionic-type sublattice with Ge (which has a larger electronegativity of 2.01 Pauli units) rather than with Co and Fe and becomes stable by donating its electrons to other elements in the alloy. Ge tries to accept electrons from other elements. The Co and displaced Fe atoms have intermediate electronegativities and occupy tetrahedral sites [9,59]. This is also in agreement with the Hume-Rothery condition of phase stability of substitutional solid solution. According to this rule, the atomic size difference between two elements should be no larger than 15% and electron negativity difference no higher than 0.4 in order to form substitutional solid solution [61–63]. In our case, the atomic-size and electronegativity difference between Fe (atomic radius 156 pm and electronegativity 1.83 Pauli units) and Cr (atomic radius 166 pm and electronegativity 1.66 Pauli units) are ∼10% and −0.11, respectively, and that between Co (atomic radius 152 pm and electronegativity 1.88 Pauli units) and Fe are ∼3% and −0.03, respectively [38,60].

Lattice parameters were calculated using Cohen's method with a Nelson-Riley extrapolation [64]. Figure 7 displays the dependence of the lattice parameter a on the Cr concentration x for $Co_{2-x}Cr_xFeGe$. It is clearly seen that the lattice parameter increases linearly with increasing chromium content. This behavior is expected from Vegard's law [65] due to the larger atomic radius of Cr (185 pm) compared with Co (152 pm) [38].

3. *Magnetic characterization*

Most of the Co-based half-metallic Heusler alloys show a Slater-Pauling-like behavior for the magnetization when crystallized in a fully ordered state [66]. The Slater-Pauling (SP) rule relates the dependence of the magnetic moment with the valence electron concentration (Z_t) following a simple electron counting scheme for ordered, half-metallic ferromagnetic Heusler compounds. If the value of the saturation magnetization changes with Cr concentration x according to the Slater-Pauling rule of thumb for half-metals, then we expect the total magnetization to be [6,9]

$$M_t = [(2-x)Z_{Co} + xZ_{Cr} + Z_{Fe} + Z_{Ge}] - 24, \qquad (1)$$

where, M_t is the total spin magnetic moment per f.u. in μ_B and Z_i is the number of valence electrons of each individual atom. In $Co_{2-x}Cr_xFeGe$ system, the total number of valence electrons change from 30 in CFG to 27 in CFVG. Therefore, the SP behavior predicts that the saturation magnetic moment

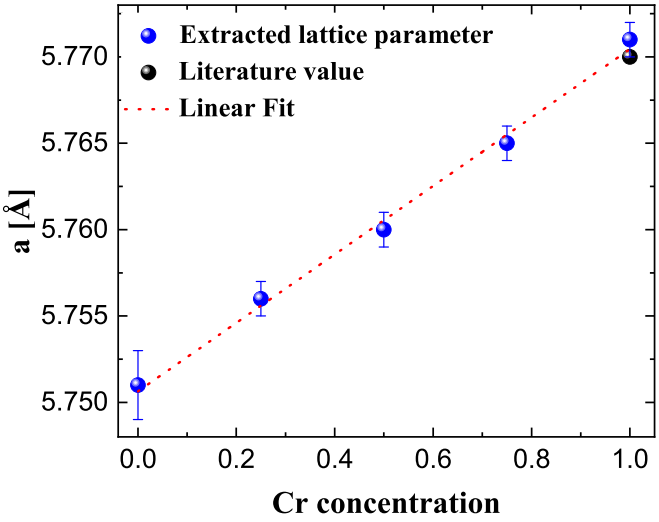

FIG. 7. Variation of lattice parameter with Cr concentration showing linear behavior. The black data point is the reported literature value [30,36].

should decrease with the partial substitution of Cr for Co. A saturation magnetic moment of

$$M(x) = 6 - 3x \tag{2}$$

is expected for $Co_{2-x}Cr_xFeGe$.

The low-temperature magnetic measurements for all single-phase alloys were done using the VSM option of a Quantum design PPMS Dynacool working in the temperature range of T = 1.8 K to 400 K and with maximum possible magnetic field of 9 T. Figure 8(a) shows the magnetization curves measured at 1.8 K (see the Supplemental Material [46] for magnetization curves at 300 K). The magnetization curves shown in Fig. 8(a) are characteristic for ferromagnets. All the alloys are saturated in magnetic field of about 5 kOe, indicating small magnetocrystalline anisotropy. All the alloys are observed to be magnetically very soft with low coercivity (H_c) of about 20 Oe [see inset to Fig. 8(a) for $x = 0.50$]. The spontaneous magnetizations (M_s) were determined from an Arrot plot [67], i.e., by linear extrapolation to H/M=0 of M^2 vs H/M curve [see inset to Fig. 8(b)]. The saturation magnetic moments deduced from the spontaneous magnetization at 1.8 K are in good agreement with those expected for Slater-Pauling half-metals (see red data points) and decrease almost linearly with the increase of Cr content [see Fig. 8(b)]. The decrease of the total saturation magnetic moment with the increase in Cr content can only be attributed to the decrease in number of Co atoms. The magnetic moment per formula unit for $x = 1$, i.e., CoFeCrGe is measured to be 3.07 μ_B, which is also in agreement with the observation of Enamullah *et al.* [36]. The slight deviation from integer value of magnetic moment could be due to the slight variation in the stoichiometry of the compounds, weighing and measurement errors, partial surface oxidation, and the measurement temperature of 1.8 K. All experimentally extracted saturation magnetic moments are also in good agreement with those obtained from first-principle calculations (see Table IV), as described in the forthcoming section. Figure 9(a) shows the temperature dependent specific magnetization of the investi-

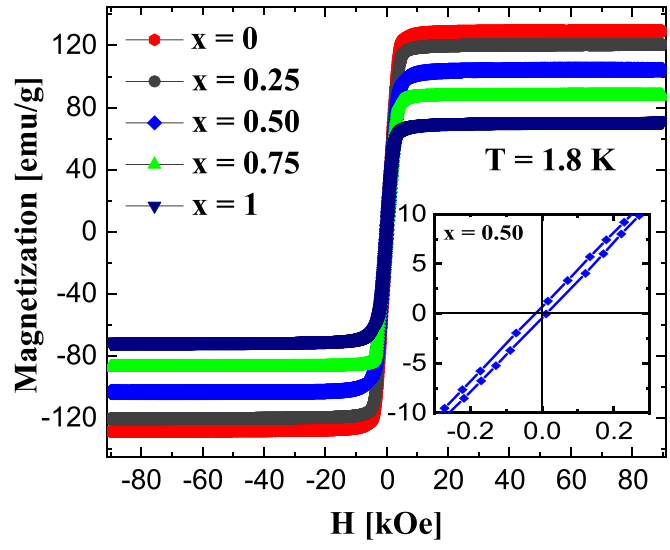

(a)

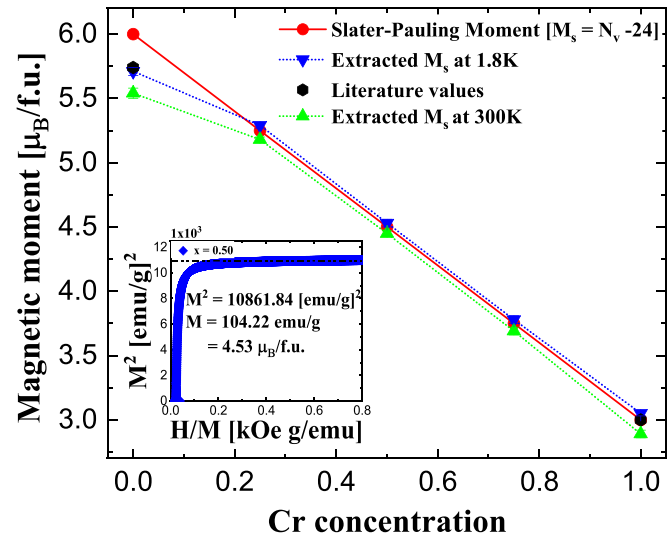

(b)

FIG. 8. (a) The field-dependent magnetization at 1.8 K of $Co_{2-x}Cr_xFeGe$ ($0 \leqslant x \leqslant 1$). The inset shows the enlargement for $x = 0.50$. (b) The saturation magnetic moment vs Cr concentration, both the experimental value and the value calculated according to the Slater-Pauling rule for half-metals.The inset shows the Arrot plot for $x = 0.50$. The black data points represent reported literature values [30,36].

gated specimens, measured by means of a vibrating sample magnetometer (LakeShore VSM 7407) equipped with a high temperature stage. The measurements were performed in a constant magnetic field of 100 Oe. The Curie temperatures of intermetallic alloy series were extracted from the inflection point, i.e., by taking the minima of the first-order derivative of M(T) curves [see inset in Fig. 9(a)]. The Curie temperature is observed to decrease with increasing Cr content due to the weakening of the exchange interaction caused by small magnetic moment of substituted Cr compared to Co. The decrease in T_c can also be attributed to the increase in lattice parameter with the substitution of Cr changing the

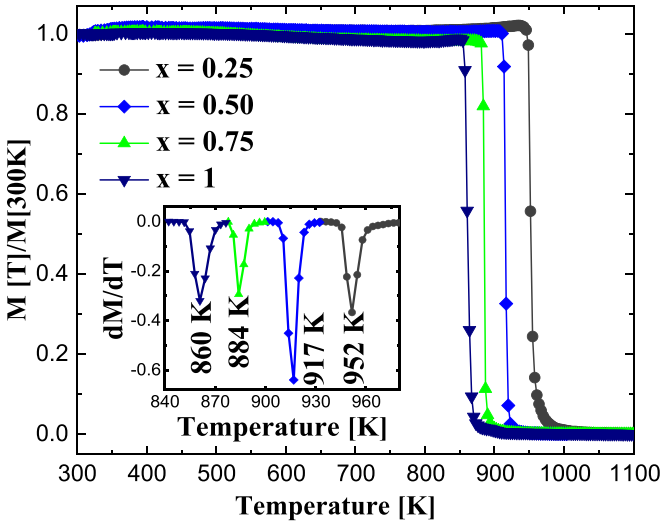

(a)

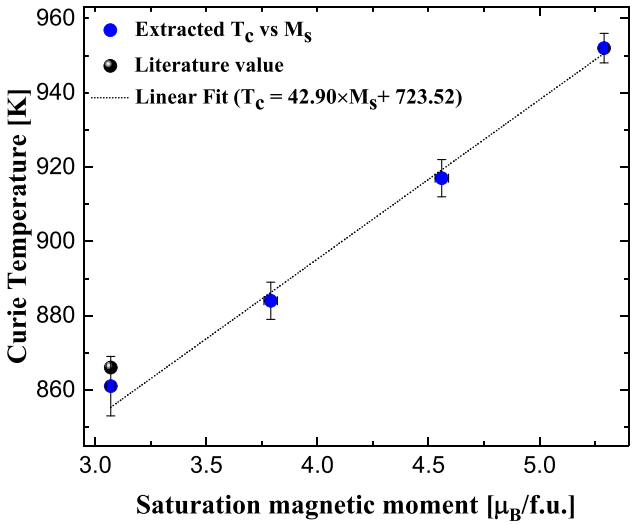

(b)

FIG. 9. (a) Temperature dependence of magnetization at 100 Oe. The inset shows the first-order derivative of magnetization as a function of temperature, the minima of which is used to extract T_c. (b) Variation of Curie temperature as a function of saturation magnetic moment.The black data points represents reported literature value [36].

distance between magnetic ions leading to a weak-exchange interaction. Compared to other low valence transition metals V and Ti, the large magnetic moment at the Cr sites due to the exchange splitting between the Cr-*d* states in the spin-up and the spin-down channels is responsible for the small variation of T_c with the increase of Cr content [31,68]. A linear dependence is obtained when plotting the Curie temperature T_c of all single-phase samples as a function of their saturation magnetic moments [see Fig. 9(b)], which is expected in half-metallic Co-based Heusler alloys [40]. According to this plot, T_c is the highest for those that exhibit a large magnetic moment, or equivalently for those with a high valence electron concentration as derived from the Slater-Pauling rule. The high values of Curie temperatures usually imply stable magnetism and half-metallicity over wide temperature range, necessary in practical applications. By extrapolating a linear dependence, T_c is estimated to be 980 K for parent Co_2FeGe ($x = 0$) in good agreement with the reported value 981 K [30].

TABLE II. Experimental lattice parameters and saturation magnetic moments at T = 1.8 K along with the Slater-Pauling (SP) values, and the measured Curie temperature (T_c) of $Co_{2-x}Cr_xFeGe$ alloy series. The numbers in parentheses are the uncertainty in the last digit, e.g., 5.29(2) = 5.29 ± 0.02.

x	Expt. lattice parameter (Å)	Expt. M_s (μ_B/f.u.)	SP (μ_B/f.u.)	T_C (K)
0[†]	a = 5.751(3)	5.71(3)	6.00	981[30]
0.25	a = 5.756(1)	5.29(2)	5.25	952(4)
0.50	a = 5.760(1)	4.53(3)	4.50	917(5)
0.75	a = 5.765(1)	3.78(3)	3.75	864(5)
1	a = 5.771(1)	3.05(2)	3.00	861(8)

[†]Multiphase specimen.

The experimentally determined lattice parameters, saturation magnetic moments at 1.8 K and corresponding Curie temperature of all single-phase samples in $Co_{2-x}Cr_xFeGe$ alloy series are summarized in Table II.

4. Vickers micro hardness

Adaptation of materials to industrial applications requires mechanical robustness to undergo repetitive thermal cycling and resist cracking from vibrations. Most of the previous studies on mechanical properties are theoretical in nature and only few are verified experimentally. The observed disconnect between the few available experimental results and the various theoretical results requires the necessity of more experimental studies in this area. Fig. 10 shows the variation of Vickers micro hardness of the alloy series with Cr concentration measured at room temperature with corresponding values in Table III. Hardness values reported are the averages of data taken from at least 12 different regions of each sample with 0.2 kg load and 10 s loading time. The Vickers hardness is

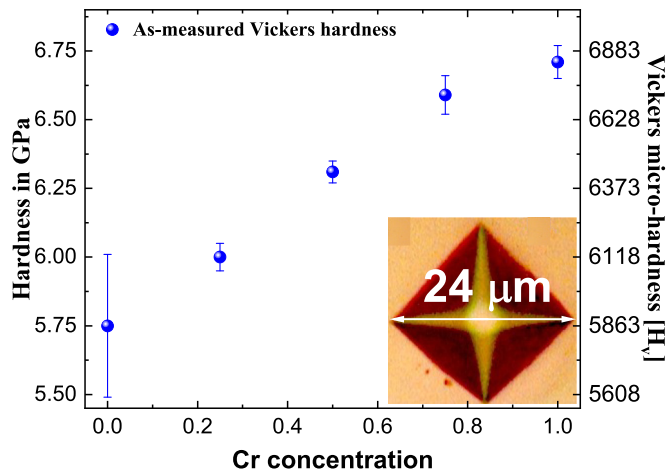

FIG. 10. Vickers hardness vs Cr concentration in $Co_{2-x}Cr_xFeGe$, all annealed at 1000 °C for 15 days, with imprint of the indenter with radial cracks for $x = 0.50$ [bottom right].

TABLE III. Vickers micro-hardness of the $Co_{2-x}Cr_xFeGe$ alloy series.

x	Vickers hardness (GPa)
0[†]	5.75 ± 0.26
0.25	6.00 ± 0.05
0.50	6.31 ± 0.04
0.75	6.59 ± 0.07
1	6.71 ± 0.06

[†]Multiphase specimen.

calculated from

$$HV = 1.8544F/D^2[\mathrm{kg/mm^2}], \quad (3)$$

where D is the diagonal length of the impression of the diamond probe. Relatively high hardness values are measured, approaching 6.71 GPa for $x = 1$, comparable to the values reported for Heuslers in the literature [31,57,69–73]. The hardness is observed to increase almost linearly with the increase of Cr concentration and depends on phases present as reported in the literature [74].

B. Theoretical results and discussions

From experiment, it is clear that the Cr substitution in Co_2FeGe stabilizes the $Co_{2-x}Cr_xFeGe$ system with XRD patterns consistent with $L2_1$ structure. But, small differences in the atomic scattering factors between the constituent $3d$-metals Co, Fe, and Cr and the unknown degree of texturing in the samples make it difficult to determine the chemical order relying only on XRD data. In order to obtain further information about the stability and chemical ordering in $Co_{2-x}Cr_xFeGe$ system, we have calculated the zero-temperature electronic structure, magnetic structure, and relative site preference energies for various possible atomic configurations, considering the symmetry of $L2_1$, Y and other disordered structures. The site preference energies of different configurations are shown in Fig. 11. The magnetic moment value is also depicted in the color axis on the right. The highlighted data points correspond to the most stable configuration (Type I in Table I). These calculations show that the higher Cr content alloys are energetically most stable. Various calculated parameters are summarized in Table IV. To describe the atomic configurations, we have used the occupation of the Wyckoff positions of space group 216 (structure Y) referring 4a and 4b sites as A sublattice and 4c and 4d as B sublattice as implemented in Ref. [31]. Before relaxation, both A and B sublattices are simple cubic with every atom on A sublattice at the center of a cube with eight B sublattice atoms at the corners and every atom on the B sublattice at the center of a cube with eight A sublattice atoms at the corners. The distortion from cubic symmetry in most of the considered configurations after relaxation to eliminate the forces on the atom is observed to be of the order of a few percents or less.

From present calculations, the configuration with Ge and Fe atoms occupying A sublattice and Co atoms on B sublattice, which is $L2_1$ structure, appear to be energetically favorable in the case of parent compound CFG ($x = 0$), consistent with the reported results [29–31,75]. However, the configuration with Co, Fe, Cr, and Ge atoms occupying 4d, 4c, 4b, and 4a sites, respectively, which is Y structure, is observed to be more stable in the case of other end member CFCG ($x = 1$), which is also consistent with reported results [34,36]. So, the crystal structure has changed as we go from one end ($x = 0, L2_1$) to the other end ($x = 1$, Y). It can also be seen that the Fe atoms can occupy 4b sites sharing the same sublattice A with Ge ($x = 0$) as well as 4c sites sharing the Co sublattice B ($x = 1$).

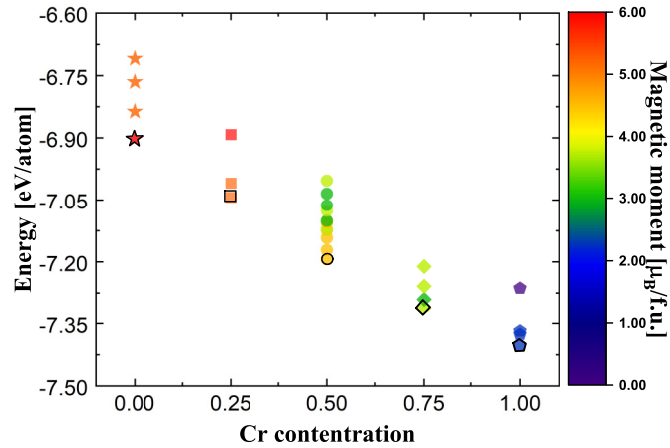

FIG. 11. Site preference energies (in eV/atom) for different configurations of $Co_{2-x}Cr_xFeGe$ as a function of Cr concentration created manually. Each data point represents a different configuration given in Table IV and the color axis indicates the magnetic moment value for each structure.

Out of different possible configurations shown in Table IV, only the configurations with Fe, Cr, and Ge on A sublattice (4a and 4b sites) and Co and Fe on the B sublattice (4c and 4d sites) appear to be energetically favourable after Cr substitution. This is consistent with the electronegativity rule as Cr is the least electronegative in the series and more likely to form an ionic-type sublattice with the most electronegative Ge rather than Fe or Co as discussed in XRD section above. In the case of $x = 0.50$, the two Cr atoms, which substitute Co atoms in the chemical formula occupy actually sites within the A sublattice (4b sites) and the two Fe atoms initially at these sites in the perfect $L2_1$ structure migrate to the B sublattice initially occupied purely by Co atoms. The displaced two Fe atoms occupy 4c and 4d sites one each together with Co atoms in B sublattice. This pattern of atoms distribution among the various sites was found to be the most favorable energetically against any other configuration, that we have considered, as shown in Table IV. The effect of Cr substitution seems to be significant on structural parameters. The computationally optimized lattice parameters are found to increase with the increase of Cr content, consistent with experimentally observed values. Due to the fact that experiments were done at a finite temperature, the experimental lattice parameters are slightly higher than those calculated from DFT (at 0 K) due to the thermal expansion coefficient of the material.

Co-based Heusler alloys are potential candidates for various spintronic applications. They usually show metallic behavior in the majority spin channel and give significant

TABLE IV. Possible atomic configurations and corresponding parameters extraced from DFT calculations. In the table E, E_0, M, M_{SP}, and $\langle a \rangle$ represent calculated energy, energy of most stable configuration, calculated magnetic moment, Slater-Pauling moment, and optimized lattice parameter. The last column shows the tetragonality in the structure.

Configurations	4d	4c	4b	4a	E–E_0 (eV)	M (μ_B/f.u.)	M–M_{SP} (μ_B/f.u.)	$\langle a \rangle$ (Å)	Tet. (a/c-1)
$x = 0$									
Co_8-Fe_4Ge_4	4Co	4Co	4Fe	4Ge	0	5.773	–0.227	5.747	0.000
Co_7Fe-Fe_3CoGe_4	4Co	1Fe,3Co	1Co,3Fe	4Ge	1.060	4.990	–1.010	5.719	0.012
Co_8-Fe_4Ge_4	4Co	4Co	3Fe,1Ge	1Fe,3Ge	2.210	5.031	–0.969	5.731	0.020
Co_7Ge-Fe_4CoGe_3	4Co	1Ge,3Co	4Fe	1Co,3Ge	3.104	4.932	–1.068	5.752	0.020
$x = 0.25$									
Co_7Fe-Fe_3CrGe_4	4Co	1Fe,3Co	1Cr,3Fe	4Ge	0	5.242	–0.008	5.753	0.000
Co_7Cr-Fe_4Ge_4	4Co	1Cr,3Co	4Fe	4Ge	0.546	5.195	–0.055	5.752	0.000
Co_7Ge-Fe_4CrGe_3	4Co	1Ge,3Co	4Fe	1Cr,3Ge	2.421	5.512	0.262	5.798	0.000
$x = 0.50$									
Co_6Fe_2-$Fe_2Cr_2Ge_4$	1Fe,3Co	1Fe,3Co	2Cr,2Fe	4Ge	0	4.500	0	5.759	0.012
Co_6Fe_2-$Fe_2Cr_2Ge_4$	4Co	2Fe,2Co	2Cr,2Fe	4Ge	0.124	4.495	–0.009	5.755	0.015
Co_4Fe_4-$Co_2Cr_2Ge_4$	4Co	4Fe	2Cr,2Co	4Ge	0.268	4.428	–0.072	5.757	0.024
Co_6Cr_2-Fe_4Ge_4	4Co	2Cr,2Co	4Fe	4Ge	0.571	4.408	–0.092	5.768	0.010
Co_5Fe_3-$CoFeCr_2Ge_4$	1Fe,3Co	2Fe,2Co	1Co,2Cr,1Fe	4Ge	0.600	4.111	–0.389	5.785	0.025
Co_6FeCr-Fe_3CrGe_4	1Fe,3Co	1Cr,3Co	1Cr,3Fe	4Ge	0.860	4.481	–0.019	5.749	0.003
Co_6Cr_2-Fe_4Ge_4	1Cr,3Co	1Cr,3Co	4Fe	4Ge	0.903	4.458	–0.043	5.787	0.020
$Co_4Fe_2Cr_2$-$Co_2Fe_2Ge_4$	4Co	2Fe,2Cr	2Fe,2Co	4Ge	0.930	3.084	–1.416	5.752	0.010
Co_5Cr_2Fe-$CoFe_3Ge_4$	1Cr,3Co	1Cr,1Fe,2Co	1Co,3Fe	4Ge	1.324	3.816	–0.684	5.702	–0.009
$Co_4Fe_2Cr_2$-$Co_2Fe_2Ge_4$	1Fe,1Cr,2Co	1Fe,1Cr,2Co	2Co,2Fe	4Ge	1.544	3.445	–1.055	5.790	0.020
$Co_4Fe_2Cr_2$-Co_4Ge_4	2Fe,1Cr,1Co	2Fe,1Cr,1Co	4Co	4Ge	1.676	3.395	–1.105	5.961	0.089
$Fe_4Co_2Cr_2$-Co_4Ge_4	2Cr,2Co	4Fe	4Co	4Ge	1.756	3.904	–0.596	5.860	0.064
$x = 0.75$									
Co_5Fe_3-$FeCr_3Ge_4$	1Fe,3Co	2Fe,2Co	3Cr,1Fe	4Ge	0	3.750	0	5.764	0.000
Co_4Fe_4-$CoCr_3Ge_4$	4Co	4Fe	1Co,3Cr	4Ge	0.326	3.124	0.626	5.708	0.001
Co_5Cr_3-Fe_4Ge_4	1Cr,3Co	2Cr,2Co	4Fe	4Ge	0.831	3.746	–0.004	5.729	–0.013
Co_5FeCr_2-$CrFe_3Ge_4$	1Cr,3Co	1Cr,1Fe,2Co	1Cr,3Fe	4Ge	1.593	3.745	0.005	5.759	0.003
$x = 1$									
Co_4Fe_4-Cr_4Ge_4	4Co	4Fe	4Cr	4Ge	0	3.000	0	5.770	0.000
Co_4Cr_4-Fe_4Ge_4	4Co	4Cr	4Fe	4Ge	0.103	2.963	–0.037	5.759	–0.007
Co_4Cr_4-Fe_4Ge_4	2Cr,2Co	2Cr,2Co	4Fe	4Ge	0.233	2.971	–0.029	5.817	0.021
Co_4Ge_4-Fe_4Cr_4	4Co	4Ge	4Fe	4Cr	2.230	0.611	–2.389	5.767	0.000

band gap in the minority spin channel. We have also simulated the spin-polarized electronic structure for most stable configurations of $Co_{2-x}Cr_xFeGe$ ($x = 0$, 0.25, 0.50, 0.75, and 1). Figure 12 shows the calculated density of states (DOS) plots for majority and minority spin channels where the Fermi level is represented by the zero energy. It can be seen clearly that the system exhibits half-metallic behavior after Cr substitution because there is finite DOS at the Fermi level in the majority spin channel, while a band gap exists in the minority spin channel. In the case of parent compound CFG [Fig. 12(a)], there is significant amount of DOS at the Fermi level on both the spin channels. After Cr substitution, the Fermi level is observed to shift deeper in energy-levels and falls at the middle of the energy gap on spin down channel for $x = 0.50$ [Fig. 12(c)]. Further increase of Cr content shifts the Fermi level towards the lower edge of energy gap due to lattice expansion as reported by Galanakis *et al.* [6]. But, still Fermi level lies within energy gap making the system half-metallic. The energy gap is observed to increase with the increase of Cr content. Computationally extracted minority spin gaps at Fermi level for $x = 0.50$, 0.75, and 1 are respectively 0.121 eV, 0.173 eV, and 0.471 eV. It can be seen clearly that the equiatomic CFCG system has a significant minority spin gap, agreeing well with the reported results [34,36]. Although, the calculated minority spin gap is the highest for $x = 1$, the half-metallic gap is greater for $x = 0.50$. Here, the half-metallic gap refers to the spin-flip gap and is the minimum between the lower edge of the conduction bands with respect to the Fermi level and the absolute value of the upper edge of the valence bands in the minority spin channel [76,77]. In $Co_{2-x}Cr_xFeGe$ alloy series, the bottom of the minority conduction bands are located at 0.041 eV, 0.145 eV, and 0.444 eV while the top of the minority valence bands at -0.080 eV, -0.028 eV, –0.027 eV for $x = 0.50$, 0.75, and 1, respectively. So, half-metallic gaps are 0.041 eV, 0.028 eV, and 0.027 eV for $x = 0.50$, 0.75, and 1, respectively.

Figure 13 shows the calculated atom-resolved DOS plots for $x = 0.50$. In predicted most stable configuration (I) (Fig. 14), it is clear that Fe(I) atoms, which share the same sublattice A with Cr, and Fe(II) atoms sharing the same sublattice B with Co have different nearest neighbor environment. Though all Co atoms occupy A sublattice, there are

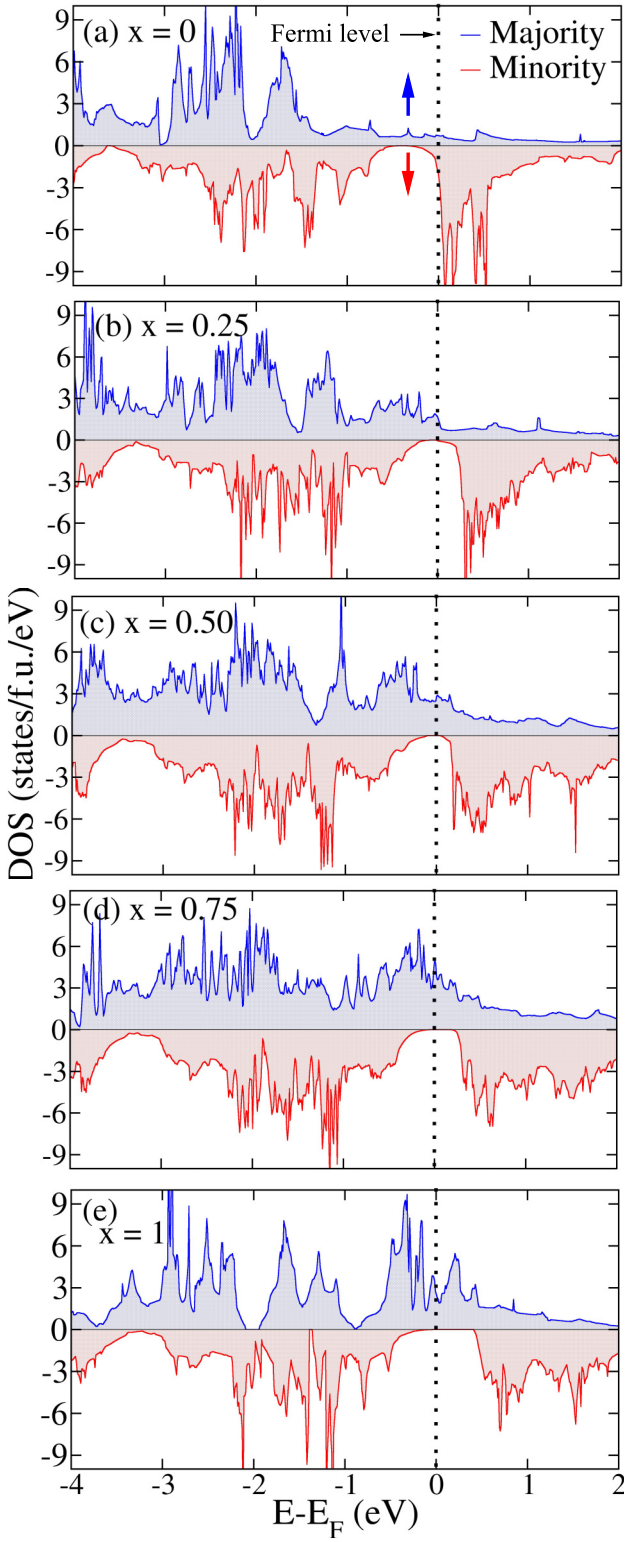

FIG. 12. Spin polarized total DOS for $Co_{2-x}Cr_xFeGe$ ($x = 0$, 0.25, 0.50, 0.75, and 1). The blue arrow represents the majority spin channel and red arrow represents minority spin channel. Number of states in each figure is scaled with respect to one formula unit.

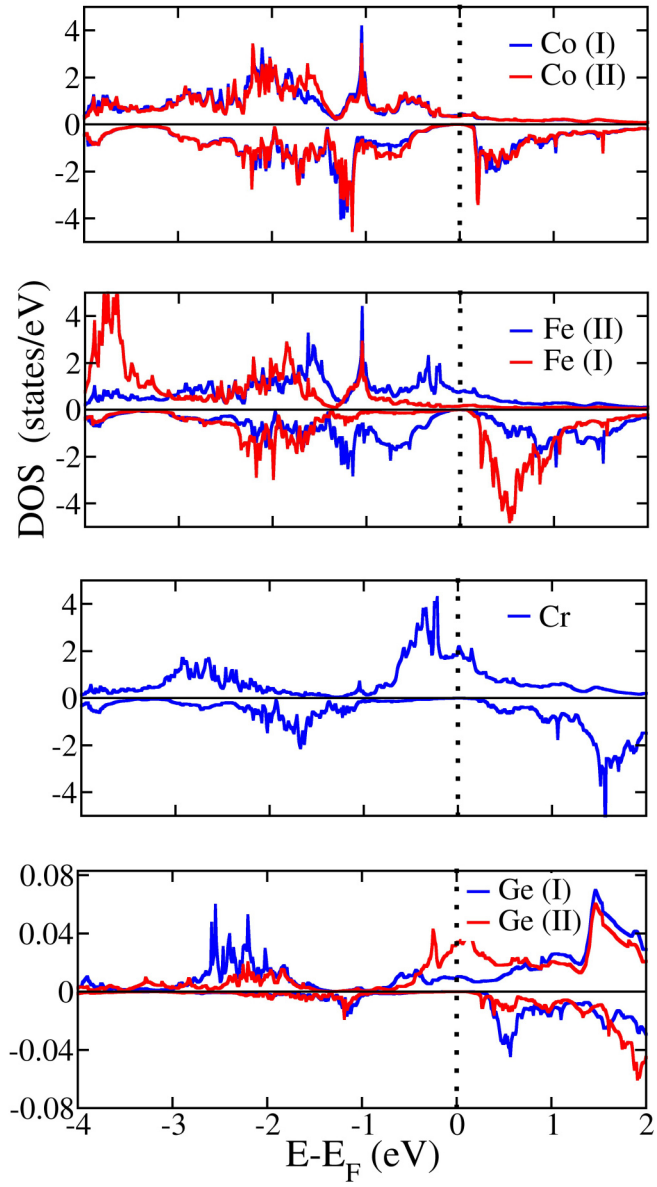

FIG. 13. Atom-resolved DOS for $x = 0.50$. I and II in parenthesis distinguishes the same atom type with different magnetic environment. For simplicity same color is used for minority (lower-half) and majority (upper-half) spin channels in each case.

two different magnetic environments due to Fe atoms, which are represented by Co(I) and Co(II) in Fig. 14. Likewise, in B sublattice, the nearest-neighbor environment of Ge(I) and Ge(II) are different, but that of two substituted Cr atoms is same. The contribution to spin-resolved DOS from same atom types with different nearest-neighbor environment is different, which is depicted in Fig. 13. Further, the atomic spin magnetic moments are calculated to be $1.027\mu_B$, $0.975\mu_B$, $2.795\mu_B$, $1.308\mu_B$ $1.964\mu_B$, $-0.063\mu_B$, and $-0.034\mu_B$ for Co(I), Co(II), Fe(I), Fe(II), Cr, Ge(I), and Ge(II), respectively. We can safely conclude that symmetry and the nearest-neighbors environment play a crucial role in the properties of the various atoms in half-metallic Heusler compounds. Co(I) and Co(II) atoms at the 4c and 4d sites have the same nearest neighbors [two Fe(I) and two Cr atoms at the 4b sites and four Ge atoms at the 4a sites] but different next-nearest neighbors. Both Co(I) and Co(II) atoms have similar DOS as shown in Fig. 13 and their atom-resolved spin magnetic moments differ by about

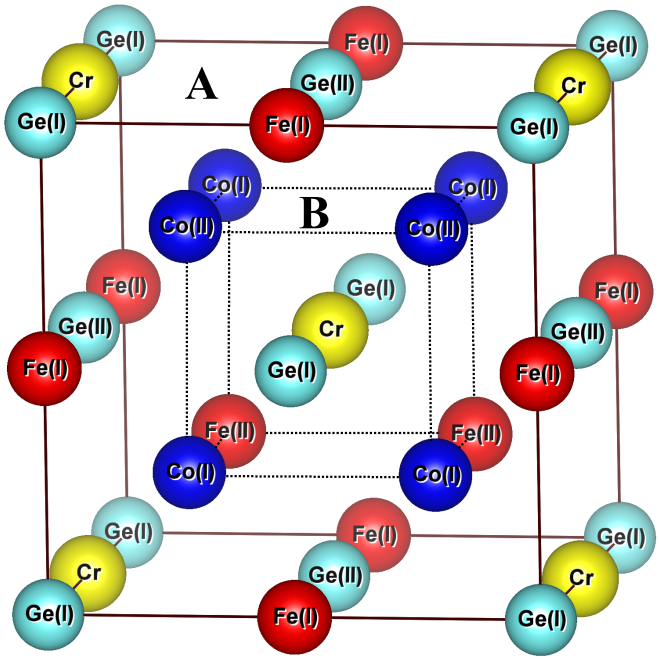

FIG. 14. Crystal structure showing the different magnetic environments in unit cell of $x = 0.50$ assuming I configuration in Table IV.

only $0.052\mu_B$. In the case of Fe atoms, the situation is more complex. Fe(I) atoms share the same sublattice A with the Cr atoms while Fe(II) atoms share the same sublattice B with the Co atoms. Thus their nearest-neighbors environment is completely different. As a result and as shown in Fig. 13 their DOS is completely different. The Fe(I) atoms present a d-DOS, which shares a lot of features with the one of the Cr atoms. There is a very large exchange splitting between majority-spin occupied and minority-spin unoccupied d-states resulting to a very large minority spin gap and a very large Fe(I) spin magnetic moment of $2.795\mu_B$, which is more than double the spin magnetic moment of the Fe(II) atoms. All $3d$ atoms in $Co_{2-x}Cr_xFeGe$ series have parallel spin magnetic moments and are ferromagnetically coupled. The details of the calculated atomic spin magnetic moments is provided within the Supplemental Material [46].

If one looks at Cr DOS in Fig. 13, it has some very nice characteristics, which make it ideal for using it as an impurity in Heusler alloys. First, there is a large exchange splitting between the occupied majority-spin and unoccupied minority-spin states. This leads to large band gaps since the conduction minority-spin states are located higher in energy with respect to the Fermi level when compared to Co or Fe atoms. Second and also very important, since Cr has less electrons than Co or Fe, the width of the majority-spin d-bands is smaller in the case of Cr and the Fermi level intersects almost the DOS peak. This leads to considerable higher majority-spin d-DOS at the Fermi level in the Cr-doped CFG compounds, which in real world means that these compounds should keep a higher degree of spin-polarization at the Fermi level.

IV. CONCLUSION

In conclusion, we performed a detailed experimental and theoretical study on the structural, electronic, magnetic, and mechanical properties of Cr-substituted Co_2FeGe Heusler alloys. The alloys are found to crystallize in the face-centered cubic structure for $0.25 \leqslant x \leqslant 1$. The isothermal magnetization curves showed that the saturation magnetic moment decreases with the increase of Cr content and the values at 1.8 K are found in good agreement with the Slater-Pauling rule of thumb for half-metals. High values of T_c, decreasing with increasing Cr substitution from 952 K for $x = 0.25$ to 861 K for $x = 1$ are measured, allowing for applications at room temperature and above. First-principles calculations predicted finite band gap in the minority spin channel, with half-metallic gaps 0.041 eV, 0.028 eV, and 0.027 eV for $x = 0.50$, 0.75, and 1, respectively. The small finite states at E_F in the minority spin channel of CFG are observed to decrease forming a finite band gap with the increase of Cr content. All these properties, with a confirmation from both theory and experiment, make $Co_{2-x}Cr_xFeGe$ Heusler alloy a promising material for spintronics application. However, experimental study of other properties such as current spin polarization is needed to confirm the above observations.

ACKNOWLEDGMENTS

We would like to acknowledge Dr. Mark Weaver for helpful discussions on measurements of mechanical properties and for providing the instrument for hardness measurements. This work utilizes the facilities offered by the Alabama Analytical Research Center (AARC) of the University of Alabama. We are thus grateful to the members of AARC for helping us with measurements. The computational resources were provided by the UA High Performance Computing Facility (UAHPC). The financial support to conduct this work was sourced from NSF DMREF Grant No. 1235396, and NSF DMR Grant No. 1508680. The authors are thankful to NSF for providing the funding support in successful completion of this work.

[1] R. A. de Groot, F. M. Mueller, P. G. van Engen, and K. H. J. Buschow, New Class of Materials: Half-Metallic Ferromagnets, Phys. Rev. Lett. **50**, 2024 (1983).

[2] T. Hahn, The 230 space groups, *International Tables for Crystallography Volume A: Space-Group Symmetry* (Springer, New York, 2006), pp. 112–717.

[3] M. J. Mehl, D. Hicks, C. Toher, O. Levy, R. M. Hanson, G. Hart, and S. Curtarolo, The AFLOW library of crystallographic prototypes: Part 1, Comput. Mater. Sci. **136**, S1 (2017).

[4] K. Buschow and P. Van Engen, Magnetic and magneto-optical properties of Heusler alloys based on aluminium and gallium, J. Magn. Magn. Mater. **25**, 90 (1981).

[5] C. Felser, G. H. Fecher, and B. Balke, Spintronics: A challenge for materials science and solid-state chemistry, Angew. Chem. Int. **46**, 668 (2007).

[6] I. Galanakis, P. Dederichs, and N. Papanikolaou, Slater-Pauling behavior and origin of the half-metallicity of the full-Heusler alloys, Phys. Rev. B **66**, 174429 (2002).

[7] C. Felser and G. H. Fecher, *Spintronics: From Materials to Devices* (Springer Science & Business Media, New York, 2013).

[8] J. Kübler, A. R. William, and C. B. Sommers, Formation and coupling of magnetic moments in Heusler alloys, Phys. Rev. B **28**, 1745 (1983).

[9] T. Graf, C. Felser, and S. S. Parkin, Simple rules for the understanding of Heusler compounds, Prog. Solid State Chem. **39**, 1 (2011).

[10] D. Kieven, R. Klenk, S. Naghavi, C. Felser, and T. Gruhn, I-II-V half-Heusler compounds for optoelectronics: *Ab initio* calculations, Phys. Rev. B **81**, 075208 (2010).

[11] S. A. Khandy and D. C. Gupta, DFT investigations on mechanical stability, electronic structure and magnetism in Co_2TaZ (Z = Al, Ga, In) Heusler alloys, Semicond. Sci. Technol. **32**, 125019 (2017).

[12] H. Mori, Y. Odahara, D. Shigyo, T. Yoshitake, and E. Miyoshi, Electronic band structure calculations on thin films of the $L2_1$ full Heusler alloys X_2YSi (X, Y = Mn, Fe, and Co): Toward spintronic materials, Thin Solid Films **520**, 4979 (2012).

[13] D. Serrate, J. De Teresa, R. Cordoba, and S. Yusuf, Magnetoresistance and magnetostriction of $Co_2Cr_{0.6}Fe_{0.4}Al$ Heusler alloy, Solid State Commun. **142**, 363 (2007).

[14] S. Picozzi, A. Continenza, and A. J. Freeman, Role of structural defects on the half-metallic character of Co_2MnGe and Co_2MnSi Heusler alloys, Phys. Rev. B **69**, 094423 (2004).

[15] S. Wurmehl, G. H. Fecher, H. C. Kandpal, V. Ksenofontov, C. Felser, and H.-J. Lin, Investigation of Co_2FeSi: The Heusler compound with highest Curie temperature and magnetic moment, Appl. Phys. Lett. **88**, 032503 (2006).

[16] K. Ziebeck and P. Webster, A neutron diffraction and magnetization study of Heusler alloys containing Co and Zr, Hf, V or Nb, J. Phys. Chem. Solids **35**, 1 (1974).

[17] P. Brown, K.-U. Neumann, P. Webster, and K. Ziebeck, The magnetization distributions in some Heusler alloys proposed as half-metallic ferromagnets, J. Phys.: Condens. Matter **12**, 1827 (2000).

[18] A. Jezierski, Magnetic properties of partially ordered $Co_{2-x}Pd_xTiSn$ alloys, J. Magn. Magn. Mater. **164**, 381 (1996).

[19] A. Yamasaki, S. Imada, R. Arai, H. Utsunomiya, S. Suga, T. Muro, Y. Saitoh, T. Kanomata, and S. Ishida, Orbital angular momentum and interpretation of core-absorption magnetic circular dichroism on the band picture in Co-based Heusler alloys Co_2YSn(Y = Ti, Zr, and Nb), Phys. Rev. B **65**, 104410 (2002).

[20] C. Felser and A. Hirohata, *Heusler Alloys* (Springer, New York, 2015).

[21] S. Karthik, A. Rajanikanth, T. Nakatani, Z. Gercsi, Y. Takahashi, T. Furubayashi, K. Inomata, and K. Hono, Effect of Cr substitution for Fe on the spin polarization of $Co_2Cr_xFe_{1-x}Si$ Heusler alloys, J. Appl. Phys. **102**, 043903 (2007).

[22] N. Tezuka, N. Ikeda, S. Sugimoto, and K. Inomata, Giant tunnel magnetoresistance at room temperature for junctions using full-Heusler $Co_2FeAl_{0.5}Si_{0.5}$ electrodes, Jpn. J. Appl. Phys. **46**, L454 (2007).

[23] B. C. S. Varaprasad, A. Rajanikanth, Y. Takahashi, and K. Hono, Enhanced spin polarization of Co_2MnGe Heusler alloy by substitution of Ga for Ge, Appl. Phys. Express **3**, 023002 (2010).

[24] T. Nakatani, A. Rajanikanth, Z. Gercsi, Y. Takahashi, K. Inomata, and K. Hono, Structure, magnetic property, and spin polarization of $Co_2FeAl_xSi_{1-x}$ Heusler alloys, J. Appl. Phys. **102**, 033916 (2007).

[25] B. Deka, A. Srinivasan, R. Singh, B. C. S. Varaprasad, Y. Takahashi, and K. Hono, Effect of Co substitution for Mn on spin polarization and magnetic properties of ferrimagnetic Mn_2VAl, J. Alloys Compd. **662**, 510 (2016).

[26] B. C. S. Varaprasad, A. Srinivasan, Y. Takahashi, M. Hayashi, A. Rajanikanth, and K. Hono, Spin polarization and Gilbert damping of $Co_2Fe(Ga_xGe_{1-x})$ Heusler alloys, Acta Mater. **60**, 6257 (2012).

[27] K. Özdoğan, B. Aktaş, I. Galanakis, and E. Şaşıoğlu, Influence of mixing the low-valent transition metal atoms (Y, Y*=Cr, Mn, Fe) on the properties of the quaternary Co_2 [$Y_{1-x}Y^*_x$] Z (Z=Al, Ga, Si, Ge, or Sn) Heusler compounds, J. Appl. Phys. **101**, 073910 (2007).

[28] I. Galanakis, K. Özdoğan, B. Aktaş, and E. Şaşıoğlu, Effect of doping and disorder on the half metallicity of full Heusler alloys, Appl. Phys. Lett. **89**, 042502 (2006).

[29] M. Kumar, T. Nautiyal, and S. Auluck, Full potential results on the magneto-optical properties of the Heusler compounds Co_2FeX (X= Al, Ga, Si and Ge), J. Phys.: Condens. Matter **21**, 196003 (2009).

[30] K. R. Kumar, K. K. Bharathi, J. A. Chelvane, S. Venkatesh, G. Markandeyulu, and N. Harishkumar, First-principles calculation and experimental investigations on full-Heusler alloy Co_2FeGe, IEEE Trans. Magn. **45**, 3997 (2009).

[31] S. KC, R. Mahat, S. Regmi, A. Mukherjee, P. Padhan, R. Datta, W. H. Butler, A. Gupta, and P. LeClair, Tunable properties and potential half-metallicity in $(Co_{2-x}Ti_x)FeGe$ Heusler alloys: An experimental and theoretical investigation, Phys. Rev. Materials **3**, 114406 (2019).

[32] B. Balke, S. Wurmehl, G. H. Fecher, C. Felser, M. d. C. M. Alves, F. Bernardi, and J. Morais, Structural characterization of the Co_2FeZ (Z= Al, Si, Ga, and Ge) Heusler compounds by x-ray diffraction and extended x-ray absorption fine structure spectroscopy, Appl. Phys. Lett. **90**, 172501 (2007).

[33] G. Gao, L. Hu, K. Yao, B. Luo, and N. Liu, Large half-metallic gaps in the quaternary Heusler alloys CoFeCrZ (Z= Al, Si, Ga, Ge): A first-principles study, J. Alloys Compd. **551**, 539 (2013).

[34] Y. Jin, P. Kharel, P. Lukashev, S. Valloppilly, B. Staten, J. Herran, I. Tutic, M. Mitrakumar, B. Bhusal, A. O'Connell *et al.*, Magnetism and electronic structure of CoFeCrX (X= Si, Ge) Heusler alloys, J. Appl. Phys. **120**, 053903 (2016).

[35] Z. Cui, B. Wu, X. Ruan, Q. Zhou, Z. Liu, X. Fu, and Y. Feng, Enhancing the half-metallicity of equiatomic quaternary Heusler compound CoFeCrGe via atomic doping, Results Phys. **15**, 102533 (2019).

[36] Enamullah, Y. Venkateswara, S. Gupta, M. R. Varma, P. Singh, K. G. Suresh, and A. Alam, Electronic structure, magnetism, and antisite disorder in CoFeCrGe and CoMnCrAl quaternary Heusler alloys, Phys. Rev. B **92**, 224413 (2015).

[37] I. Galanakis, P. H. Dederichs, and N. Papanikolaou, Origin and properties of the gap in the half-ferromagnetic heusler alloys, Phys. Rev. B **66**, 134428 (2002).

[38] https://periodictable.com/Properties/A/AtomicRadius.v.html.

[39] N. Tezuka, N. Ikeda, F. Mitsuhashi, and S. Sugimoto, Improved tunnel magnetoresistance of magnetic tunnel junctions with Heusler $Co_2FeAl_{0.5}Si_{0.5}$ electrodes fabricated by molecular beam epitaxy, Appl. Phys. Lett. **94**, 162504 (2009).

[40] G. H. Fecher, H. C. Kandpal, S. Wurmehl, C. Felser, and G. Schönhense, Slater-Pauling rule and Curie temperature of Co_2-based Heusler compounds, J. Appl. Phys. **99**, 08J106 (2006).

[41] K. Kobayashi, R. Umetsu, R. Kainuma, K. Ishida, T. Oyamada, A. Fujita, and K. Fukamichi, Phase separation and magnetic properties of half-metal-type $Co_2Cr_{1-x}Fe_xAl$ alloys, Appl. Phys. Lett. **85**, 4684 (2004).

[42] R. Y. Umetsu, K. Kobayashi, A. Fujita, K. Oikawa, R. Kainuma, K. Ishida, N. Endo, K. Fukamichi, and A. Sakuma, Half-metallic properties of $Co_2(Cr_{1-x}Fe_x)Ga$ Heusler alloys, Phys. Rev. B **72**, 214412 (2005).

[43] Y. Miura, K. Nagao, and M. Shirai, Atomic disorder effects on half-metallicity of the full-Heusler alloys $Co_2(Cr_{1-x}Fe_x)Al$: A first-principles study, Phys. Rev. B **69**, 144413 (2004).

[44] I. Galanakis, Appearance of half-metallicity in the quaternary Heusler alloys, J. Phys.: Condens. Matter **16**, 3089 (2004).

[45] B. Venkateswarlu, P. Midhunlal, P. Babu, and N. H. Kumar, Magnetic and anomalous electronic transport properties of the quaternary Heusler alloys $Co_2Ti_{1-x}Fe_xGe$, J. Magn. Magn. Mater. **407**, 142 (2016).

[46] See Supplemental Material at http://link.aps.org/supplemental/10.1103/PhysRevB.104.014430 for further details on sample preparation, metallography procedures; additional optical and SEM imaging for microstructure and composition analysis; figures illustrating structural prototypes; additional magnetic characterization; more detailed theoretical results for calculated spin magnetic moments.

[47] C. Boudias and D. Monceau, *CaRIne Crystallography: The Crystallographic Software for Research and Teaching* (CaRIne Crystallography, Senlis, France, 2006).

[48] P. LeClair, X-ray diffraction calculation software, available at http://pleclair.ua.edu/XRD/.

[49] A. Putz and H. Brandenburg, MATCH!: Phase identification from power diffraction, Crystal Impact Kreuzherrenstr. 102, 53227 Bonn, Germany, https://www.crystalimpact.de/match/.

[50] P. E. Blöchl, Projector augmented-wave method, Phys. Rev. B **50**, 17953 (1994).

[51] G. Kresse and J. Furthmüller, Efficient iterative schemes for ab initio total-energy calculations using a plane-wave basis set, Phys. Rev. B **54**, 11169 (1996).

[52] J. P. Perdew, K. Burke, and M. Ernzerhof, Generalized Gradient Approximation Made Simple, Phys. Rev. Lett. **77**, 3865 (1996).

[53] H. J. Monkhorst and J. D. Pack, Special points for Brillouin-zone integrations, Phys. Rev. B **13**, 5188 (1976).

[54] P. Mavropoulos, I. Galanakis, V. Popescu, and P. Dederichs, The influence of spin-orbit coupling on the band gap of heusler alloys, J. Phys.: Condens. Matter **16**, S5759 (2004).

[55] H. S. Nalwa, *Handbook of Nanostructured Materials and Nanotechnology* (Academic Press, New York, 1999).

[56] M. Che and J. C. Védrine, *Characterization of Solid Materials and Heterogeneous Catalysts: From Structure to Surface Reactivity* (John Wiley & Sons, Hoboken, NJ, 2012).

[57] R. Mahat, K. Shambhu, D. Wines, F. Ersan, S. Regmi, U. Karki, R. White, C. Ataca, P. Padhan, A. Gupta, and P. LeClair, Tuneable structure and magnetic properties in $Fe_{3-x}V_xGe$ alloys, J. Alloys Compd. **830**, 154403 (2020).

[58] P. Webster, Magnetic and chemical order in Heusler alloys containing cobalt and manganese, J. Phys. Chem. Solids **32**, 1221 (1971).

[59] T. J. Burch, T. Litrenta, and J. I. Budnick, Hyperfine Studies of Site Occupation in Ternary Systems, Phys. Rev. Lett. **33**, 421 (1974).

[60] https://periodictable.com/Properties/A/Electronegativity.an.html.

[61] W. Hume-Rothery, Researches on the nature, properties, and conditions of formation of intermetallic compounds, with special reference to certain compounds of tin, Ph.D. thesis, University of London, 1926.

[62] A.-P. Tsai, A test of Hume-Rothery rules for stable quasicrystals, J. Non-Cryst. Solids **334**, 317 (2004).

[63] M.-x. Ren, B.-s. Li, and H.-z. Fu, Formation condition of solid solution type high-entropy alloy, Trans. Nonferrous Met. Soc. China **23**, 991 (2013).

[64] B. Cullity and S. Stock, *Elements of X-ray Diffraction* (Addison-Wesley, New York, 2014).

[65] A. R. Denton and N. W. Ashcroft, Vegard's law, Phys. Rev. A **43**, 3161 (1991).

[66] T. Block, M. J. Carey, B. A. Gurney, and O. Jepsen, Band-structure calculations of the half-metallic ferromagnetism and structural stability of full- and half-Heusler phases, Phys. Rev. B **70**, 205114 (2004).

[67] A. Arrott, Criterion for ferromagnetism from observations of magnetic isotherms, Phys. Rev. **108**, 1394 (1957).

[68] S. H. Aly and R. M. Shabara, First principles calculation of elastic and magnetic properties of Cr-based full-Heusler alloys, J. Magn. Magn. Mater. **360**, 143 (2014).

[69] M. Hakimi, P. Kameli, H. Salamati, and Y. Mazaheri, Evolution of microstructural and mechanical properties of nanocrystalline Co_2FeAl Heusler alloy prepared by mechanical alloying, Powder Metall. **56**, 111 (2013).

[70] S. Ouardi, G. H. Fecher, B. Balke, A. Beleanu, X. Kozina, G. Stryganyuk, C. Felser, W. Klöß, H. Schrader, F. Bernardi, J. Morais, E. Ikenaga, Y. Yamashita, S. Ueda, and K. Kobayashi, Electronic and crystallographic structure, hard x-ray photoemission, and mechanical and transport properties of the half-metallic Heusler compound Co_2MnGe, Phys. Rev. B **84**, 155122 (2011).

[71] R. Mahat, Shambhu KC, D. Wines, S. Regmi, U. Karki, Z. Li, F. Ersan, J. Law, C. Ataca, V. Franco *et al.*, Influence of Cr-substitution on the structural, magnetic, electron transport, and mechanical properties of $Fe_{3-x}Cr_xGe$ Heusler alloys, J. Magn. Magn. Mater. **521**, 167398 (2021).

[72] R. Mahat, K. Shambhu, U. Karki, S. Regmi, J. Y. Law, V. Franco, I. Galanakis, A. Gupta, and P. LeClair, Structural, electronic, magnetic, and mechanical properties of $Co_{2-x}V_xFeSi$ Heusler alloys, IEEE Transactions in Magnetics (2021), doi: 10.1109/TMAG.2021.3081466.

[73] R. Mahat, S. KC, D. Wines, S. Regmi, U. Karki, F. Ersan, C. Ataca, A. Gupta, and P. LeClair, Effect of V substitution on structural, magnetic, transport and mechanical properties of the

half-metal-type Heusler alloy Co_2FeGe, *APS March Meeting 2020: Novel Functional Magnetic Materials and Structures* (Bulletin of the American Physical Society, New York, 2020), Vol. 62, abstract: M35.00002.

[74] G. Rogl, A. Grytsiv, M. Gürth, A. Tavassoli, C. Ebner, A. Wünschek, S. Puchegger, V. Soprunyuk, W. Schranz, E. Bauer *et al.*, Mechanical properties of half-Heusler alloys, Acta Mater. **107**, 178 (2016).

[75] D. P. Rai, A. Shankar, Sandeep, M. P. Ghimire, and R. K. Thapa, A comparative study of a Heusler alloy Co_2FeGe using LSDA and LSDA+ U, Phys. B: Condens. Matter **407**, 3689 (2012).

[76] K. Yao, G. Gao, Z. Liu, and L. Zhu, Half-metallic ferromagnetism of zinc-blende CrS and CrP: A first-principles pseudopotential study, Solid State Commun. **133**, 301 (2005).

[77] X. Wang, Z. Cheng, J. Wang, L. Wang, Z. Yu, C. Fang, J. Yang, and G. Liu, Origin of the half-metallic band-gap in newly designed quaternary Heusler compounds ZrVTiZ (Z= Al, Ga), RSC Adv. **6**, 57041 (2016).